IEEE Access
Multidisciplinary ⋮ Rapid Review ⋮ Open Access Journal

Received 5 September 2023, accepted 21 September 2023, date of publication 25 September 2023,
date of current version 28 September 2023.

Digital Object Identifier 10.1109/ACCESS.2023.3318871

RESEARCH ARTICLE

Four-Arm Log-Periodic Toothed Antenna With Hybrid Reflector Composed of Inhomogeneous Metamatarial Elements for Electronic Support Measures

DONGHYUN KIM, CHAN YEONG PARK, (Graduate Student Member, IEEE), CHANG-HYUN LEE, AND YOUNG JOONG YOON, (Senior Member, IEEE)

Electrical and Electronic Engineering Department, Yonsei University, Seoul 03722, Republic of Korea
Radar Research and Development Laboratory, LIG Nex1 Company Ltd., Yongin-si 16911, Republic of Korea

Corresponding author: Young Joong Yoon (yjyoon@yonsei.ac.kr)

This work was supported by the Challenging Future Defense Technology Research and Development Program of Agency for Defense Development, in 2019, under Grant 9127786.

ABSTRACT A novel method of enhancing radiation performance is demonstrated by applying a hybrid reflector composed of inhomogeneous metamaterial elements to a four-arm log-periodic toothed antenna. The operation of the antennas by various metamaterial cells is observed, and the causes of the radiation performance deterioration and narrow bandwidth are investigated through the field distribution analysis. The metamaterial cells are arranged in suitable positions under the antenna for good radiation performance and wide bandwidth according to AMC and EBG characteristics. In the proposed hybrid reflector, surface wave suppression characteristics are used for impedance stabilization by placing the I-shaped EBG cell under the inactive region of the antenna. The performance of the fabricated antenna with dual linear polarization capability is verified by measuring co- and cross-polarization radiation patterns. The newly proposed hybrid reflector for the four-arm log-periodic toothed antenna represents an over 4 dBi realized gain within an impedance ratio bandwidth of over 11.6:1.

INDEX TERMS Four-arm LP-toothed antenna, electronic support measures, wide gain bandwidth, metamaterial, high impedance surface, artificial magnetic conductor, electromagnetic bandgap.

I. INTRODUCTION

The four-arm log-periodic (LP)-toothed antennas, one of the frequency-independent (F.I.) antennas, are used in various applications [1], [2], [3]. In particular, unlike spiral antennas, they have dual-linear polarization capability, making them compelling candidates for electronic support measures (ESM) systems [4], [5]. According to [6], the ESM system's receiver antenna can obtain better performance with dual-linear polarization than circular polarization capability. There are various microstrip antennas (monopole, bowtie, and tapered slot antenna etc.) that have UWB frequency response in a wide band with dual polarization capability, but it is very difficult to have both high gain and a uniform radiation pattern within a very high ratio bandwidth (10:1 or more). Considering these points, the LP-toothed antenna is the most useful candidate. In addition, unlike sinuous antennas that can operate similarly, the planar LP-toothed antenna can be fed through the integrated balun [3], [7]. This structure is very simple to manufacture and does not increase the antenna's overall height.

The planar four-arm LP-toothed antenna has been studied extensively, but most have been conducted only with a single radiator generating a bidirectional radiation pattern. To be applied to the ESM system, a unidirectional pattern and a frequency response of high efficiency and high gain is

The associate editor coordinating the review of this manuscript and approving it for publication was Debabrata K. Karmokar.

required over a very wide frequency range covering the electronic warfare (EW) band. In particular, the antenna gain is a major determinant of the ESM system performance, more important than reflection coefficient characteristics. In addition, a wide gain bandwidth helps reduce the number of antennas mounted in the system. These unidirectional radiation patterns and gain enhancement have studied through various reflector structures. The electric conductor reflector is efficient in a narrow band but cause instability in the frequency response of the reflection coefficient and radiation performance in the wide band [8]. Therefore, additional absorbing materials are usually used [10], [11]. However, using absorbers loses the radiation efficiency near the low-frequency band of these antennas. These problems can be solved by expanding the antenna profile, but conceptually, the radiation efficiency cannot be more than 50%.

Studies have used various metamaterial structures as a reflector to overcome these shortcomings [12], [13], [14], [15], [16], [17], [18], [19], [20], [21], [22], [23], [24]. In [12], [13], and [14], vialess rectangular high-impedance surface (HIS) cells are homogeneously placed under the outer edge of the antenna to realize artificial magnetic conductor (AMC) characteristics, thereby realizing a unidirectional pattern even in a low-profile structure. However, improving radiation performance is insufficient due to the narrow bandwidth of the AMC characteristics. As a more improved method, there is a structure that enhances the radiation performance in a wider band through a multi-layered HIS reflector [15], [16] or a multi-resonance HIS reflector [17], [18], [19], [20]. However, these structures still have narrow impedance bandwidth and non-uniform radiation performance. This is due to frequency response fluctuation of impedance because of its complex structure.

There have been studies on mushroom-liked cell reflectors using electromagnetic bandgap (EBG) characteristics to overcome these limitations [21], [22], [23], [24]. The EBG reflector has a relatively stable frequency response of antenna performance within the operating band. In addition, these metamaterial reflectors have low-profile structures. However, in antennas that use EBG characteristics, antenna radiation performance deterioration is observed near the EBG band. The impedance bandwidth is still narrow compared to the absorber-filled cavity-backed structures, making them unsuitable for ESM systems [25]. Like the various types of reflectors mentioned above, high gain and wide gain bandwidth cannot be achieved through these simple structures. Moreover, since most of the studies using various metamaterial cells such as HIS and EBG together with antennas lack accurate comparison of operating principles and characteristics above the reflector, research on this is necessary.

In this paper, various HIS and EBG cells were placed under a planar LP-toothed antenna to observe the operation and radiation performance of each antenna. The changes in the field distribution should be analyzed in relation to the

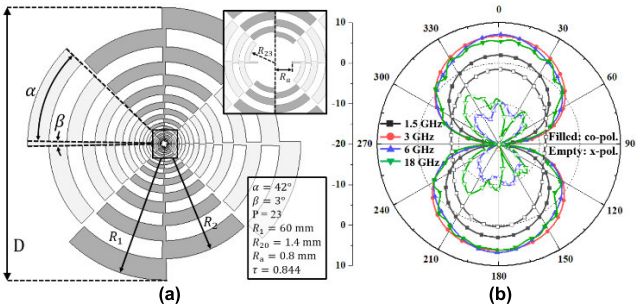

FIGURE 1. The conventional planar LP-toothed antenna: (a) configuration. (b) radiation patterns.

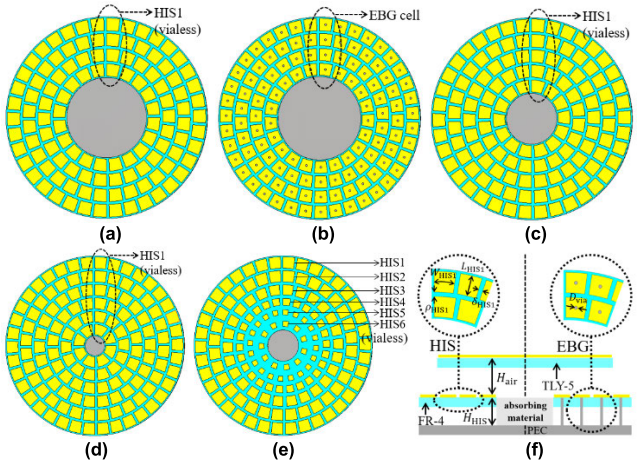

FIGURE 2. The configuration of the reflectors: (a) HIS (4-rings), (b) the EBG surface (4-rings), (c) HIS (5-rings), (d) HIS (6-rings), (e) inhomogeneous HIS (6-rings), and (f) the side view of the antenna. Design parameters: $\mathbf{H_{air}} = \mathbf{6.5}$, $\mathbf{H_{HIS}} = \mathbf{8.5mm}$.

frequency response of the antenna performance to address the previously reported problems for the wideband antennas. Through this, the metamaterial cells designed for the purpose were arranged to the appropriate locations under the radiator for improved gain bandwidth. The analysis results were verified by the measured results of the fabricated antenna and compared with similar studies.

II. DESIGN OF FOUR-ARM LP-TOOTHED ANTENNA WITH METAMATERIAL REFLECTORS

The four-arm LP-toothed antenna's configuration and radiation patterns is shown in Fig. 1. The basic design starts with the outermost teeth's length and decreases logarithmically as it goes inside by the scaling factor. The outermost teeth correspond to a quarter of the cut-off frequency wavelength [7]. The conventional antenna has a design parameter of 120 mm in diameter. In addition, a Taconic substrate ($\varepsilon_r = 2.2$, $\tan\delta = 0.0009$, h = 0.254 mm) with low relative permittivity is used to maintain stable antenna performance in a relatively high-frequency band. The reflectors are designed with a relatively high permittivity FR4 substrate ($\varepsilon_r = 4.4$, $\delta = 0.019$, h = 1.53 mm) to obtain a smaller size of the metacells compared to the antenna teeth.

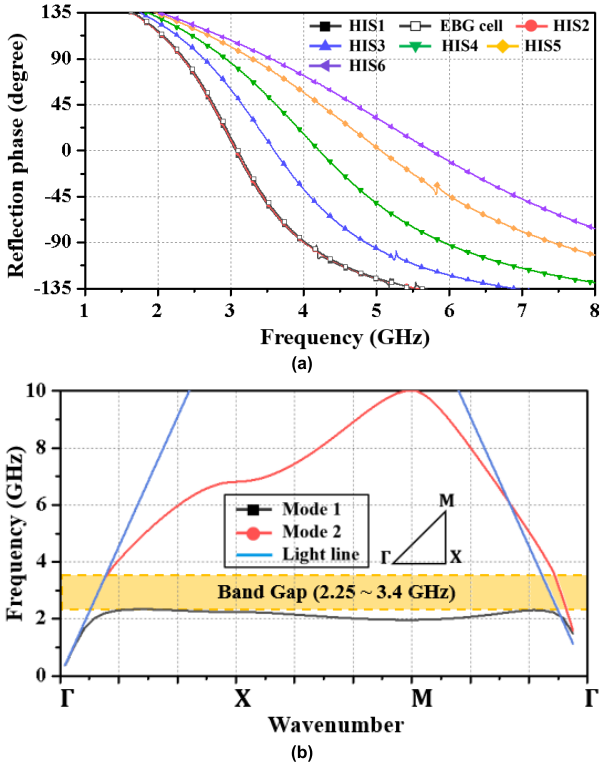

FIGURE 3. (a) Frequency response of the reflection phase for designed metamaterial cells. (b) dispersion diagram for the designed EBG cell.

A. DESIGN OF THE ANTENNA WITH METAMATERIAL REFLECTORS

Fig. 2 shows the configurations of metamaterial reflectors located 6 mm below the designed four-arm LP-toothed antenna. The same patch cells within 150 mm diameter were arranged 4–6 rings and designed for accurate comparison according to the frequency band [Figs. 2. (a), (c), and (d)]. These homogeneous vialess HIS elements constitute the reflector. Also, the mushroom-liked cell reflector is applied to observe the antenna performance for the EBG characteristics [Fig. 2(b)]. The cells designed this way were named HIS1 and EBG cells, respectively. In addition, considering the active region of the LP antenna, an inhomogeneous HIS reflector with different reflection phases according to each location was designed [Fig. 2(e)]. The parameters of the designed metamaterial elements are presented in Appendix Section. As the distance between the cells increases, the reflection phase of the designed elements shifts the AMC band to the higher band [Fig. 3(a)]. The reflection phases of HIS1 and EBG cells used in Figs. 2 (a) and (b), respectively, are almost the same. The dispersion for the EBG cells shows that the EBG occurs at 2.25–3.4 GHz [Fig. 3(b)]. The designed cell's EBG is similar to the band showing the AMC characteristics (2.25–3.4 GHz).

The frequency response of the reflection coefficient for the designed antennas is shown in Fig. 4. The performance of the cavity filled only with the absorbing material (ECCSORB LS–24) is also shown as a gray line for accurate comparison

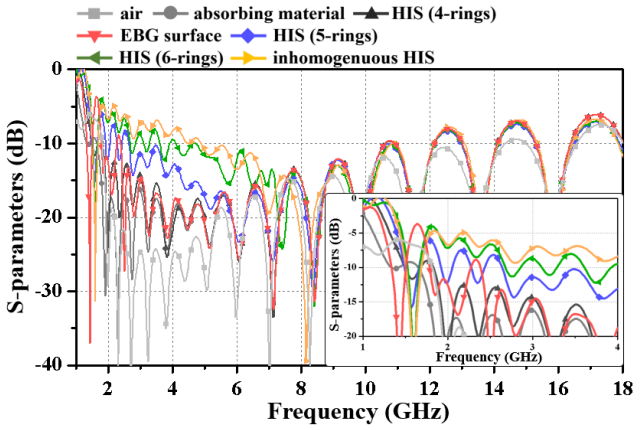

FIGURE 4. The frequency response of the reflection coefficient for the designed antennas (reference impedance 200 Ω).

with commonly used structures. In the frequency response of the reflection coefficient, the HIS (4-ring), the EBG surface, and the absorbing material were very stable and showed similar results. However, as the metamaterial cell area expanded inward, the frequency response fluctuations of the impedance increased, adversely affecting the operation of the antenna. The inhomogeneous HIS had the largest fluctuation in the entire band, and expanding the area of the cells in this way for bandwidth improvement may have caused problems in the antenna performance. These fluctuations occurred because the electric field was not only generated in the outermost teeth of the antenna, which is an active region in the low-frequency band, but also distributed near the center of the antenna [26]. These low-frequency electric fields experienced diffuse reflection as facing the cells with different reflection phases.

The radiation performance for the designed antennas is shown in Fig. 5. As opposed to the frequency response of the reflection coefficient, the internally expanded HIS reflectors had higher radiation efficiency over the entire band. The realized gains of HIS (5-rings) and HIS (6-rings) were reduced from 4 GHz or higher due to the reflection phase mismatch. On the other hand, considering the active region, the inhomogeneous HIS showed the widest gain bandwidth and good radiation efficiency. In addition, it should be noted that severe deterioration in the antenna gain and the radiation efficiency occurred near the EBG of the antenna above the EBG surface, as reported in [21]. This deterioration causes performance problems in the low-frequency band and causes bandwidth limitations. The observed results indicate that the stable reflection coefficient and improved radiation performance cannot be obtained simultaneously with only one type of metamaterial cells and their uniformity change.

B. ANALYSIS THROUGH OBSERVATION OF THE SIMULATED FREQUENCY RESPONSE AND FIELD DISTRUBUTION

The schematic electric field distribution near the cut-off frequency is shown in Fig. 6 (a) to determine the cause

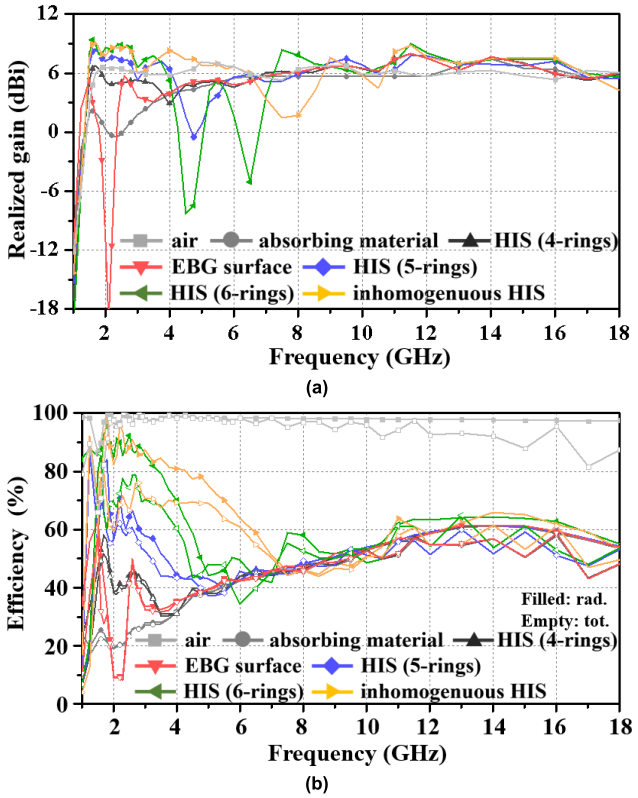

FIGURE 5. The frequency response of (a) the realized gain and (b) the efficiency for the designed antennas.

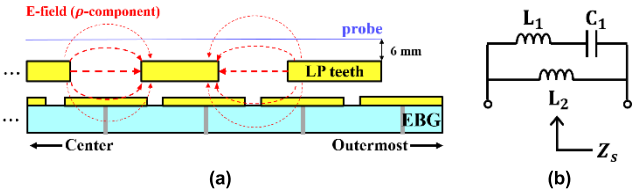

FIGURE 6. (a) Schematic electric field distribution of the four-arm LP-toothed antenna on the EBG surface. (b) Equivalent circuit model of the AMC reflector.

of the antenna deterioration on the EBG surface observed previously. This is a partial side section view to show the electric field distribution between the radiating conductors (teeth of LP-toothed antenna) on the EBG surface, and the red dotted lines represent the electric field. The electric field distributions are in opposite directions because of the out-phased current distribution between odd or even elements within the active region of the LP-toothed antenna [27]. Also, the blue line at 6 mm above the LP-toothed antenna is a probe for measuring this electric field distribution magnitude. In addition, an equivalent circuit model of the AMC reflector is shown in Fig. 6 (b), and the surface impedance (Z_s) characteristics is calculated [28]. The AMC reflector consists of a series of inductive (L_1) and capacitive layers (C_1). Between the antenna and the AMC reflector is equalized through inductance (L_2). Hence, resonant frequency f_r to

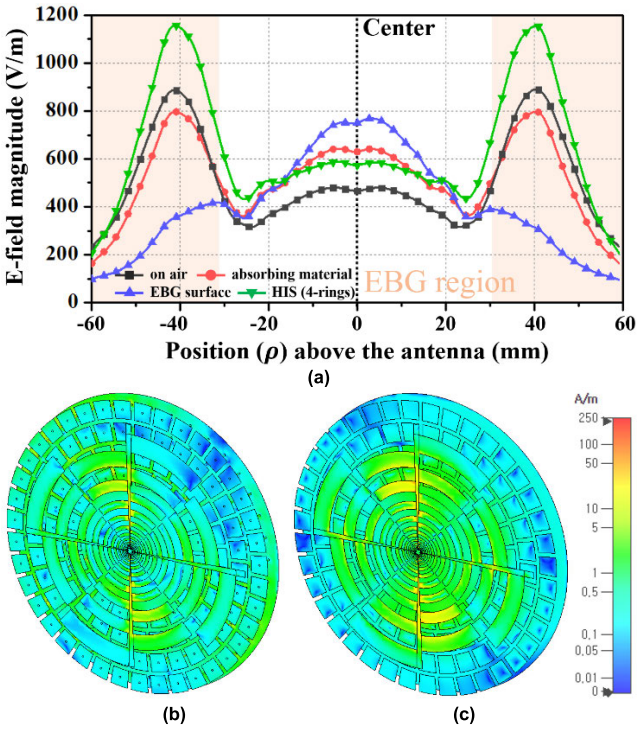

FIGURE 7. (a) The electric field distribution in the absolute value 6 mm above the antenna at 2.25 GHz. Surface current distribution at 2.25 GHz: (b) EBG surface and (c) HIS (4-rings).

generate constructive interference can be expressed as [29]

$$f_r = \frac{1}{2\pi\sqrt{(L_1 + L_2)\,C_1}} \tag{1}$$

The radiation mechanism using a reflector includes three processes: incident, reflected electromagnetic field, and coupling process. The electric field distribution from this probe above the designed antennas was observed at 2.25 GHz [Fig. 7 (a)]. The magnitude of the field distribution above the EBG surface was suppressed within the EBG region compared to the other reflectors. This phenomenon was caused by the surface wave suppression characteristics of EBG cells. This electric field suppression allowed the antenna to have a very stable reflection coefficient near the EBG band. The surface current distribution can be observed more clearly and differentiated according to the reflectors [Fig 7. (b)]. It was confirmed that the surface current is distributed even to the center of the antenna in addition to the active area, the most suppressed current distribution was confirmed on the EBG surface. The suppressed distribution of these currents does not contribute to an effective coupling process. Comparing this result with the efficiency in Fig. 5, it is confirmed that the suppressed electric field distribution at the EBG surface caused the deterioration of the realized gain and the radiation efficiency. HIS (4-rings) and the EBG surface's cells have almost the same reflection phase, but the EBG surface located close to the radiator suppresses even the electric field distribution near the active area due to the surface wave suppression characteristics. Conversely,

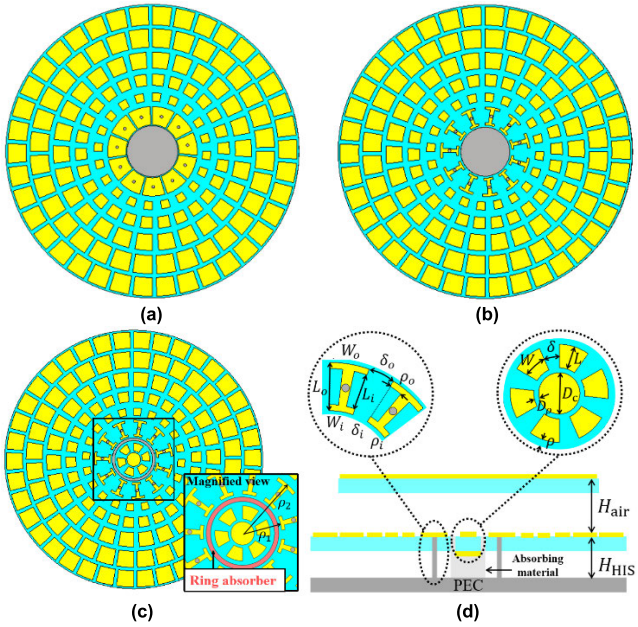

FIGURE 8. The configuration of the hybrid reflectors composed of inhomogeneous metamaterial elements: (a) the additional EBG cell, (b) the I-shaped cell, (c) the I-shaped cell & center HIS & annular ring, and (d) the side view of the antenna.

the electric field distribution magnitude above the HIS (4-ring), which was more amplified than the conditions above the absorbing material indicates improved radiation performance. Due to the current reflection of the AMC reflector with zero phase shift, the field magnitude current is reproduced and effectively participates in the coupling process. This is confirmed by the better gain and radiation efficiency above the reflectors than above the absorbing material (Fig. 5). Therefore, the HIS cells were located below the active region, which could be used to improve the radiation performance.

III. DESIGN OF THE HYBRID REFLECTOR COMPOSED OF INHOMOGENEOUS METAMATERIAL ELEMENTS

Fundamentally, the EBG characteristic is a band in which all modes are not supported by consecutive cells. Conversely, vialess HIS cells do not have these characteristics in the desired band. This is the reason why reflectors composed only of vialess HIS cells in the previous section have high gain properties but unstable impedance characteristics. Therefore, in this section, surface wave suppression characteristics are used for impedance stabilization by placing EBG cells only in the inactive region of the radiator. Consisting of inhomogeneous metamaterial elements, this hybrid reflector differs from previous studies in that it uses HIS and EBG cells together on a single PCB plane. As the first comparative reflector, Fig. 8(a) shows a reflector in which the HIS6, used in the inhomogeneous HIS [Fig. 2(e)], was replaced with the mushroom-liked cell used in the EBG surface [Fig 2(b)].

Furthermore, in Section II, it was observed that the HIS cells were more efficient in being located below the active region suitable for each AMC band. Accordingly, to improve the radiation performance, the I-shaped cells with the EBG characteristic in the low-frequency band and the AMC characteristic close to HIS6 were designed. For this characteristics, the concept of a circular non-uniform planar EBG cell was adopted. For this EBG cell mounted on a dielectric with permittivity ϵ_r, the design equations are given by [20], [30]

$$L = \mu_0 h \tag{2}$$

$$C = \frac{\epsilon_0 (1+\epsilon_r)}{\pi} \cosh^{-1}\left(\frac{w+g}{g}\right)\left[\rho_2 \ln\left(\frac{\rho_2}{\rho_1}\right) - \rho_2 + \rho_1\right] \tag{3}$$

$$f_0 = \frac{1}{2\pi\sqrt{LC}} \tag{4}$$

where ρ_1 and ρ_2 are the inner and outer radii of these EBG cells, w is the patch width, and g is the spacing between cells. Since the cell is designed as a planar structure, the height h of the cell is fixed and the inductance L is also fixed. Based on the design equation presented above, the I-shaped EBG cell with AMC characteristics at higher frequency band with low capacitance in the co-polarized direction (φ–direction) of the LP-toothed antenna is proposed. The designed I-shaped cell represents AMC characteristics in the φ-direction from 3.2–7 GHz [Fig. 9(a)]. In addition, the dispersion diagram for this cell showed the EBG characteristic occurrence at 2.25–2.7 GHz, similar to the AMC band (2.25–3.45 GHz) of the designed mushroom-liked EBG cell. As the second comparative, the additional EBG cells were replaced with the designed I-shaped cells, as shown in Fig. 8(b).

In addition, in order to improve the radiation performance in the high frequency band, a structure in which HIS cells are further expanded to the inside is proposed [Figs. 8 (c), (d)]. However, in order to implement a planar reflector suitable for a planar radiator, it has a relatively high height (8.5 mm) because it must be designed based on the low frequency band (near 2 GHz) of the outermost cell. Such a relatively high cell height has limitations in showing AMC in a high frequency band no matter how much the cell size is reduced [20]. To solve this problem, the height of the center HIS cells was reduced to 1.53 mm. The band showing the AMC characteristics of the designed center-HIS appeared in the 10.2–13.5 GHz range [Fig. 9(a)]. However, this height-changed structure can have side effects, such as unwanted EBG generation or coupling between the via of the I-shaped cell and the ground of the center-HIS cell. In addition, in the 7–10.2 GHz band, which is not covered by the AMC band of each cell, the reflection phase is 120 degrees on average, making it difficult to generate constructive interference (to increase the gain). Adjacent cells (I-shaped EBG and center HIS) having such a large difference in reflection phase cause electromagnetic field cancellation. These problems are solved by placing a ring absorber between adjacent cells (which corresponds to the theoretical active region in the 7–10.2 GHz band). In addition, an annular ring was

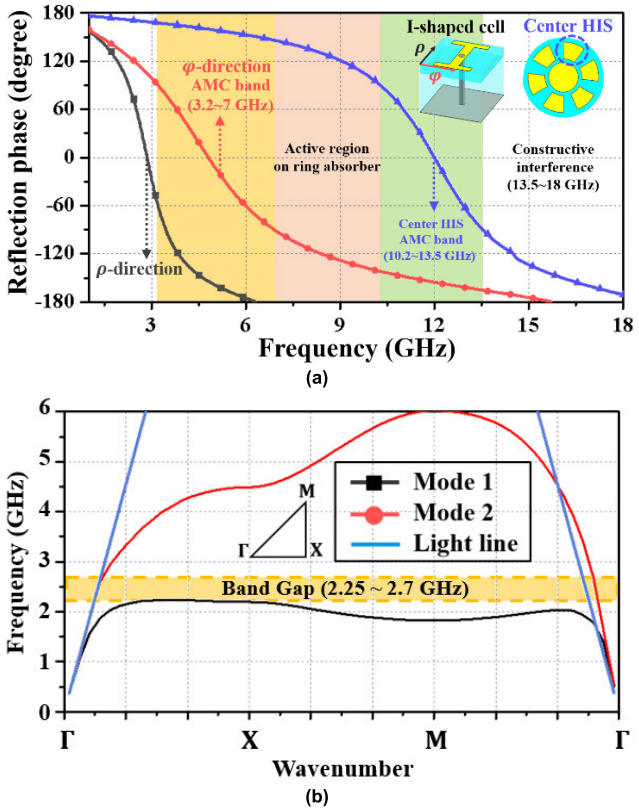

FIGURE 9. (a) The frequency response of the reflection phase for designed I-shaped and center-HIS cells. (b) The dispersion diagram for the designed I-shaped cell.

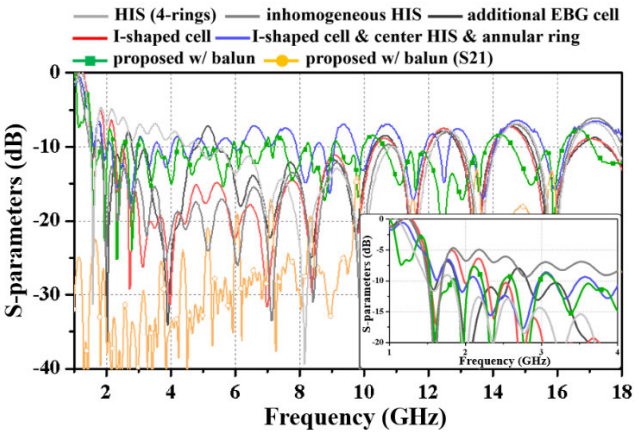

FIGURE 10. The frequency response of the reflection coefficient for the hybrid reflector antennas. (reference impedance 200 Ω).

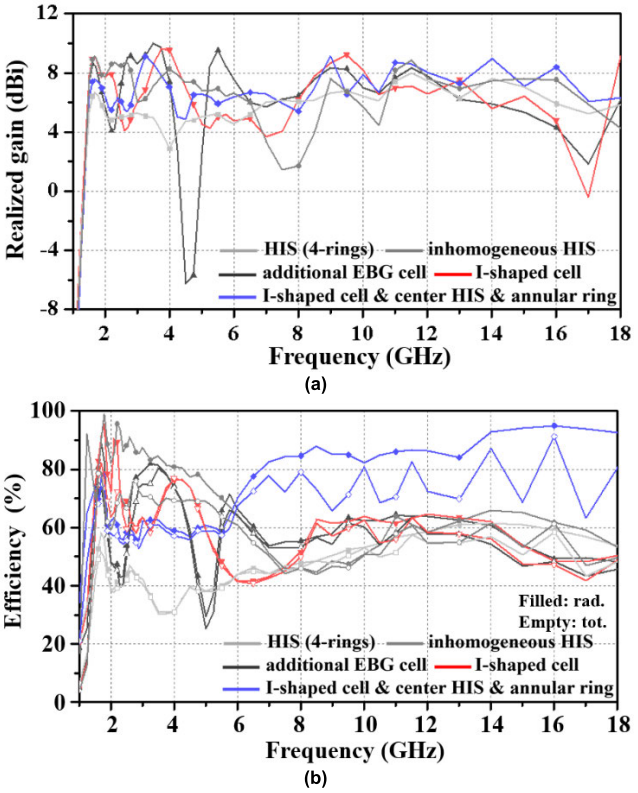

FIGURE 11. (a) The frequency response of (a) the realized gain and (b) the efficiency for the hybrid reflector antennas.

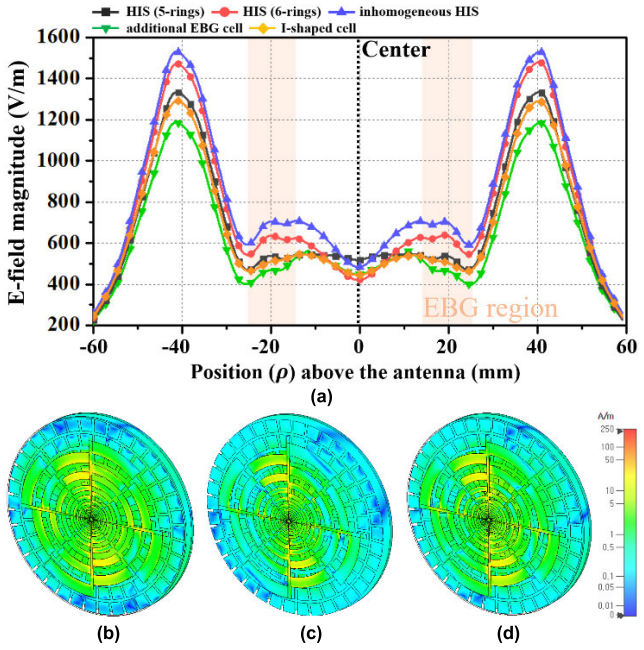

FIGURE 12. (a) the electric field distribution in the absolute value 6 mm above the antenna at 2.25 GHz. Surface current distribution at 2.25 GHz: (b) inhomogeneous HIS, (c) additional EBG, and (d) I-shaped EBG.

mounted on the outermost part of the antenna to stabilize the impedance of the low-frequency band [3].

The frequency response of the reflection coefficient for the designed hybrid reflectors is shown in Fig. 10. The additional EBG and I-shaped cells had relatively stable reflection coefficients in the entire band. Both antennas showed reflection coefficients of less than −7.5 dB at 1.8–18 GHz and 2.2–18 GHz, respectively, with a reference impedance of 200 Ω. At this particular location, the EBG cells suppressed the diffuse reflection in the low-frequency band and helped stabilize the input impedance. In particular,

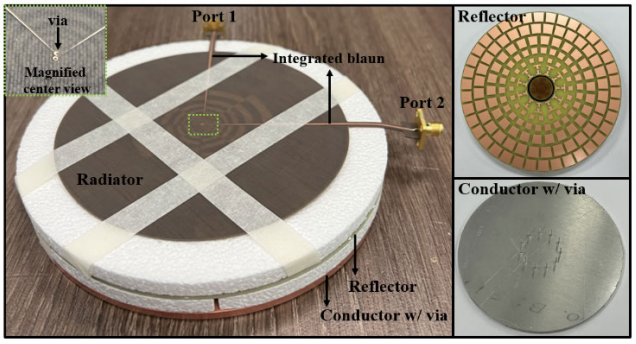

FIGURE 13. Photograph of the fabricated antenna.

the reflector with an I-shaped cell, center HIS, and annular ring showed a reflection coefficient of less than −7.5 dB from 1.5 to 18 GHz. To determine the feasibility of the proposed antenna structure, the reflection coefficient and inter-port isolation characteristics including balun (50–200 Ω) are also presented. The reflection coefficient of the proposed antenna is less than –7.5 dB, and the inter-port isolation is less than –14 dB in all bands. The realized gain of the additional EBG cell was relatively high in the low-frequency band. However, the expected deterioration occurred due to a phase mismatch near 4.5 GHz [Fig 11(a)]. On the other hand, the reflectors with center HIS showed the realized gain of more than 5 dBi at a ratio bandwidth of 12:1. Similarly, the radiation and total efficiency of the additional EBG cell had a relatively large fluctuation, while the I-shaped cell and center HIS represented more than 54% in the entire band. In particular, a very high radiation efficiency of about 80% or more was observed from 7 GHz and above. These results address the problem of low radiation efficiency in conventional cavities filled only with absorbing materials. The impedance matching of the antennas observed in Section II (4-rings HIS, EBG surface, and 5-rings HIS) is better than that of the proposed antenna. Nevertheless, in the operating band observed in this study (1–18 GHz), the proposed antenna has higher gain, efficiency, and wider gain bandwidth. Therefore, the proposed antenna is more efficient for ESM systems.

Simulations were performed to determine the electric field distribution to verify the method of locating the EBG cell under the inactive region. The absolute electric field distribution value at 6 mm above the designed antennas is observed at 2.25 GHz, including the EBG band of the designed cells [Fig. 12 (a)]. The field distributions of HIS (6-rings) and inhomogeneous HIS reflectors are relatively large in all areas. As observed in the previous section, the frequency response of the input impedance of these reflectors is very unstable. These large periodic antennas are required that the coupling process become effectively only above the active region. The shaded region (where HIS6 is located) of the inhomogeneous HIS reflector with the most unstable input impedance represents a relatively high magnitude of electric field distribution, which causes diffuse reflection. Conversely, the electric field distribution of the additional

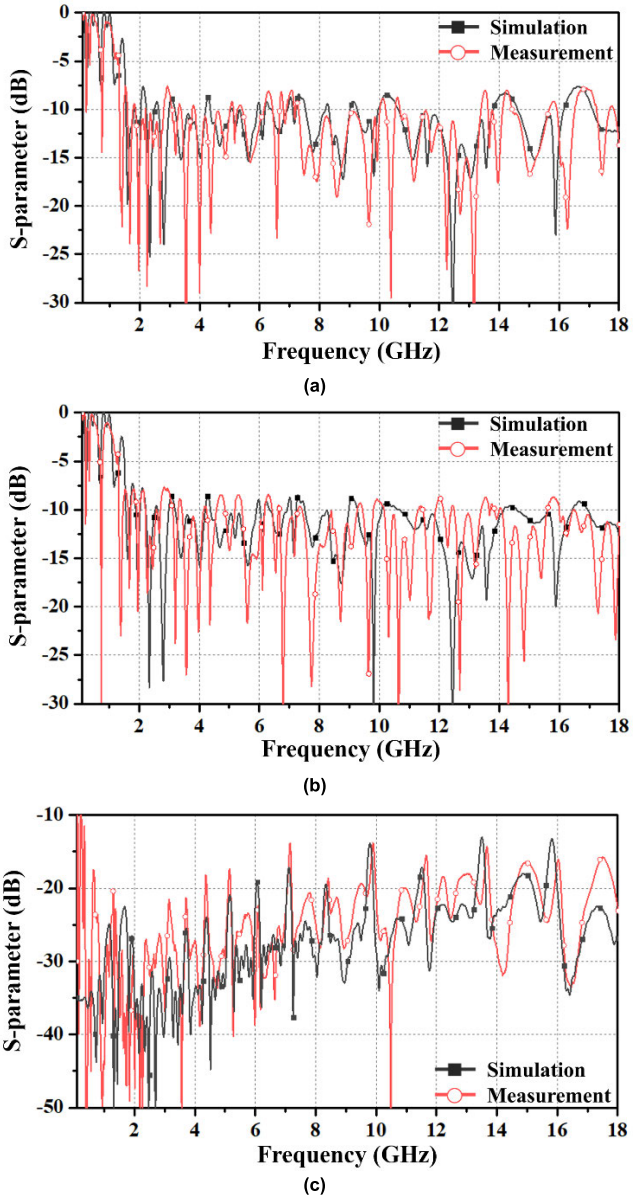

FIGURE 14. The simulated and measured scattering marameters for the proposed antenna. Reflection coefficient: (a) port-1 and (b) port-2. (c) transmission coefficient.

EBG cell and the I-shaped cell reflectors was lowered in the shaded EBG region (inactive region), and surface wave suppression was observed. The diffuse reflection reduced by the suppressed surface wave made the antenna have relatively good reflection coefficient characteristics. In addition, in the case of the inhomogeneous HIS reflector, the surface current distribution represents strongly up to the center of the antenna due to the internally expanded cells, which causes impedance fluctuations [Fig. 12. (b)]. However, when the EBG cells are located inside the inactive area [Figs. 12. (c) and (d)], the inner surface current distribution becomes smaller and the impedance is stabilized. In addition, the proposed I-shaped EBG reflector maintains high gain with stronger coupling process than the 4-rings HIS reflector in the active area.

TABLE 1. Comparison with similar works.

Ref.	Antenna type	Reflector type	−7.5 dB Ratio -impedance bandwidth	Gain	Ratio -gain bandwidth (more than 2.5 dBi)	Diameter / height (λ_L)
[12]	2-arm spiral	Rectangular HIS	10:1 (1–10 GHz)	1–7 dBi	3.57:1 (2.8–10 GHz)	0.32 / 0.04
[13]		Rectangular HIS	10:1 (0.6–6 GHz)	-2–8 dBi	4.2:1 (1–4.2 GHz)	0.29 / 0.03
[14]		Rectangular HIS	1.31:1 (1.1–1.45 GHz)	3–7.79 dBi	1.27:1 (1.14–1.45 GHz)	0.73 / 0.09
[15]		Rectangular HIS (Dual-layered)	3.33:1 (3–10 GHz)	> 5.5 dBi	2.5:1 (4–10 GHz)	0.64 / 0.1
[16]		Rectangular HIS (Dual-layered)	5:1 (2–10 GHz)	6–9 dBi	3.33:1 (3–10 GHz)	0.4 / 0.11
[17]		Inhomogeneous HIS	3.33:1 (3–10 GHz)	> 2.7 dBi	1.3:1 (6–7.8 GHz)	0.64 / 0.1
[18]		Inhomogeneous HIS	3.57:1 (2.8–10 GHz)	7.1–9.2 dBi	3.33:1 (3–10 GHz)	0.56 / 0.08
[19]		Inhomogeneous HIS	N/A	2.5–9.5 dBi	1.54:1 (6.5–10 GHz)	N/A
[20]		Inhomogeneous HIS	2:1 (0.4–0.8 GHz)	1.5–7.5 dBi	2:1 (0.4–0.8 GHz)	0.95 / 0.1
[21]		Rectangular EBG	5:1 (2–10 GHz)	3–9.5 dBi	3.33:1 (3–10 GHz)	1 / 0.06
[22]		Rectangular HIS and EBG (Dual-layered)	3.33:1 (3–10 GHz)	4.2–5.1 dBi	3.12:1 (3.2–10 GHz)	1.54 / 0.09
[23]		Rectangular EBG	3.33:1 (3–10 GHz)	4.5–9.5 dBi	3.33:1 (3–10 GHz)	1.67/ 0.09
[24]		Rectangular EBG	1.55:1 (10.3–16 GHz)	9 dBi	N/A	0.93 / 0.02
This work	4-arm LP-toothed	Rectangular HIS and EBG (single-layered)	11.6:1 (1.55–18 GHz)	4–7.6 dBi	11.6:1 (1.55–18 GHz)	0.78 / 0.08

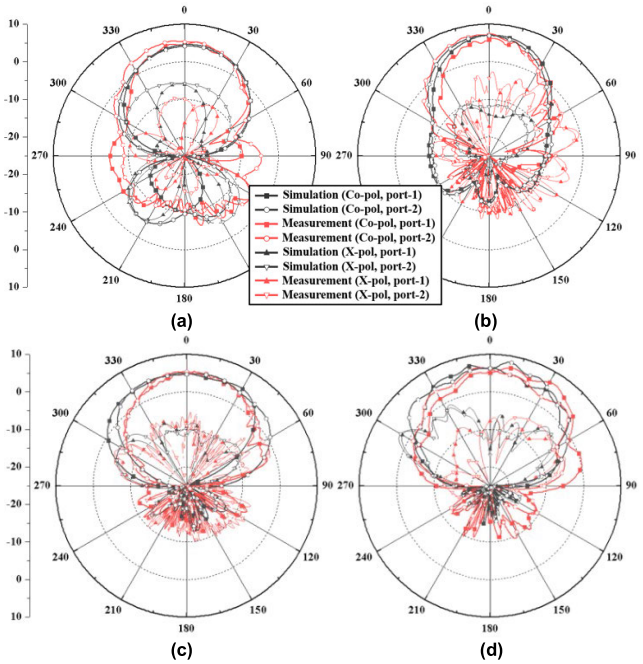

FIGURE 15. Simulated and measured radiation patterns for the proposed antenna at (a) 1.5 GHz, (b) 3 GHz, (c) 6 GHz, and (d) 18 GHz.

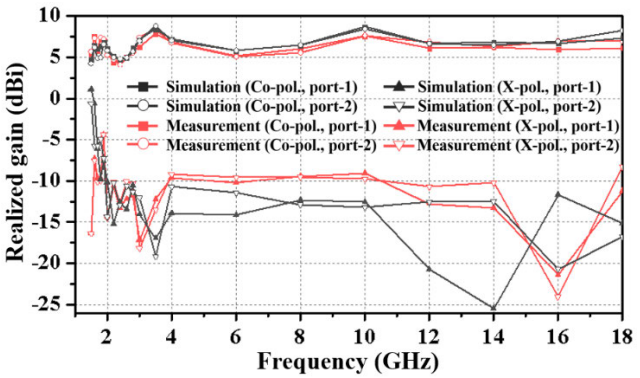

FIGURE 16. Simulated and measured realized gains in the broadside direction for the proposed antenna.

IV. SIMULATED AND MEASUREMENT RESULTS

An LP-toothed antenna designed to experimentally verify the improved radiation performance was fabricated (Fig. 13). The two-port integrated balun was used for the feeding structure for measurement [3], [7]. This integrated balun was designed and fabricated with an impedance transition of 50–200 Ω. The line width of the integrated balun at the center of the antenna is 0.04 mm, and the diameter of the via for connection is 0.4 mm. The reflection coefficient measurement result appears in the 1.55–18 GHz band range based on −7.5 dB (Fig. 14). The transmission coefficient is −13 dB or less in all bands. The total diameter of the antenna was 150 mm, and the electrical length based on the measured results was 0.78 λ_L at 1.55 GHz. The total height of the antenna is 15 mm, and the electrical length is 0.078 λ_L. The radiation patterns were measured at 1.5, 3, 6, and 18 GHz (Fig. 15). The realized gain in the broadside direction based on the simulated and measured results is shown in Fig. 16. The proposed antenna operates over 4 dBi in the entire band with dual linear polarization. The measured results achieved a gain ratio bandwidth (>2.5 dBi) of 11.6:1 and cross-polarization isolation of less than −13 dB in the frequency range above 1.55 GHz, which was very similar to the simulation results.

Table 1 summarizes the antenna performances of similar works. To date, only there has been a two-arm spiral type of frequency-independent antenna in which a known metamaterial-added reflector is used. Although the diameter of the four-arm LP-toothed antenna is more than twice that of the spiral antenna at the same cut-off frequency, the proposed antenna has an electrical length similar to or smaller than other references. The impedance bandwidth was compared on

TABLE 2. Design parameters of the homogeneous reflector.

Parameter	W (mm)	L (mm)	δ (mm)	ρ (mm)	Number of cells
1^{st} *ring*	9.45	9.45	2	2	38
2^{nd} *ring*	9.36	9.36	2	2	32
3^{rd} *ring*	9.25	9.25	2	2	26
4^{th} *ring*	9.11	9.11	2	2	20
5^{th} *ring*	8.93	8.93	2	2	14
6^{th} *ring*	8.65	8.65	2	-	8
D_{via}	1.5 mm				

TABLE 3. Design parameters of the inhomogeneous reflector.

Parameter	W (mm)	L (mm)	δ (mm)	ρ (mm)	Number of cells
1^{st} *ring*	9.45	9.45	2	2	38
2^{nd} *ring*	9.36	9.36	2	2.5	32
3^{rd} *ring*	8.25	8.25	3	3	26
4^{th} *ring*	5.82	5.82	3	3.75	26
5^{th} *ring*	4.22	4.22	4.5	6.25	20
6^{th} *ring*	2.39	2.39	8	-	11

TABLE 4. Design parameters of the hybrid reflectors.

Parameter	W (mm)	L (mm)	δ (mm)	ρ (mm)	Number of cells
Additional EBG cell	9.39	9.39	2	2	11
I-shaped cell (outer)	7.82	9.39	5.25	2.57	11
I-shaped cell (inner)	4.61	7	3.1	1.74	
7^{th} *ring*	4.56	4.56	3	1.5	6
D_c	1.5 mm		D_ρ	1 mm	

the boundary of −7.5 dB or less of the reflection coefficient. In addition, the proposed antenna has a relatively wide impedance ratio bandwidth, and the gain ratio bandwidth is approximately three times larger. This ratio bandwidth difference means that the proposed antenna is advantageous in improving the performance of the ESM system over other antennas.

V. CONCLUSION

In this study, we proposed a hybrid reflector composed of inhomogeneous metamaterial elements applied to the four-arm LP-toothed antenna with a wide bandwidth. Various metacells were arranged in suitable positions under the antenna according to AMC and EBG characteristics to maintain good radiation performance. The antenna radiation deterioration was identified and resolved through the field distribution change analysis. The newly proposed hybrid reflector for the four-arm LP toothed antenna represented a realized gain of over 4 dBi within an impedance ratio bandwidth of over 11.6:1. This design was also experimentally verified with dual linear polarization capability, and the proposed antenna will be a good candidate for ESM systems.

APPENDIX DETAILED DESIGN OF THE METAMATERIAL CELLS

The metamaterial cells used in this study are basically designed in a fan-shaped structure with a maximum diameter of 150 mm. In the HIS (4, 5, 6-rings) and EBG cell reflectors used in Section II, the same patch cells are arranged in 4–6 rings [Figs. 2. (a), (b), (c), and (d)]. The outermost fan-shaped array is named the first ring. The design parameters of the cells belonging to each ring are presented in Fig. 2. (e) and their values are presented in Table 2. In the inhomogeneous HIS reflector in Section II, 6 types of different patch cells are arranged in 6-rings. Likewise, the design parameters of the cells belonging to each ring are presented in Table 3. The hybrid reflectors used in Section III are the same as the inhomogeneous HIS reflector up to the 5th ring, but are different from the 6th ring (Fig. 8). The design parameters for the additional EBG cell, I-shaped cell, and center HIS cells used are presented in Table 4.

REFERENCES

[1] R. Duhamel and D. Isbell, "Broadband logarithmically periodic antenna structures," in *Proc. IRE Int. Conv. Rec.*, vol. 5, Mar. 1957, pp. 119–128.

[2] R. Sammeta and D. S. Filipovic, "Reduced size planar dual-polarized log-periodic antenna for bidirectional high power transmit and receive applications," *IEEE Trans. Antennas Propag.*, vol. 62, no. 11, pp. 5453–5461, Nov. 2014.

[3] D. Kim, C. Y. Park, and Y. J. Yoon, "Miniaturized four-arm log-periodic toothed antenna with wide bandwidth," *IEEE Antennas Wireless Propag. Lett.*, vol. 21, no. 4, pp. 745–749, Apr. 2022.

[4] C. Viswanadham, "A practical approach for controlling the shape of the radiation pattern of a microwave log-periodic antenna for wideband applications," *IEEE Antennas Propag. Mag.*, vol. 56, no. 5, pp. 304–314, Oct. 2014.

[5] A. J. Booysen, D. E. Baker, and M. D. Plessis, "AN 18–40 GHz SCAB on' spiral antenna for enhanced ESM systems," *Trans. South Afr. Inst. Electr. Engineers*, vol. 88, no. 3, pp. 112–115, Sep. 1997.

[6] R. G. L. D. Mello and C. Junqueira, "Polarization diversity on ESM systems," *J. Microw., Optoelectron. Electromagn. Appl.*, vol. 16, no. 1, pp. 273–283, Mar. 2017.

[7] H. Zhou, Y. Wang, Y.-C. Lee, and D. S. Filipovic, "Dual-polarized K/Ka-band planar log-periodic antenna," in *Proc. 6th Eur. Conf. Antennas Propag. (EUCAP)*, Mar. 2012, pp. 1–4.

[8] C. Djoma, X. Begaud, A. C. Lepage, S. Mallégol, and M. Jousset, "Wideband reflector for Archimedean spiral antenna," in *Proc. 6th Eur. Conf. Antennas Propag. (EUCAP)*, Mar. 2012, pp. 776–780.

[9] I. M. Alotaibi, J. Hong, and S. K. Almorqi, "Cavity-backed dual linear polarization sinuous antenna with integrated microstrip balun feed," in *Proc. IEEE 15th Medit. Microw. Symp. (MMS)*, Nov. 2015, pp. 1–4.

[10] E. S. Sakomura, D. B. Ferreira, I. Bianchi, and D. C. Nascimento, "Compact planar two-arm compound spiral antenna for L-/X-band direction finding applications," in *Proc. IEEE Int. Symp. Antennas Propag. USNC/URSI Nat. Radio Sci. Meeting*, Jul. 2018, pp. 853–854.

[11] Y. Yan and Q. Cao, "Microwave absorbing properties of sinuous antenna filled with absorbing material," in *Proc. IEEE Int. Conf. Ultra-Wideband*, vol. 1, Sep. 2010, pp. 1–4.

[12] C. Liu, Y. Lu, C. Du, J. Cui, and X. Shen, "The broadband spiral antenna design based on hybrid backed-cavity," *IEEE Trans. Antennas Propag.*, vol. 58, no. 6, pp. 1876–1882, Jun. 2010.

[13] Z. Wang, K. Karathanasis, and J. L. Volakis, "Axial ratio reduced ultra wideband slot spiral on hybrid impedance surfaces," *J. Electromagn. Waves Appl.*, vol. 29, no. 2, pp. 143–153, Jan. 2015.

[14] T. Yang, J. Ren, R. Q. Xi, P. C. Li, and Y. Z. Yin, "A low-profile circularly polarized antenna based on a circularly symmetric high impedance surface," *Int. J. RF Microw. Comput.-Aided Eng.*, vol. 31, no. 11, Nov. 2021, Art. no. e22821.

[15] M. Tanabe, "A spiral antenna above a hybrid HIS-EBG reflector," in *Proc. IEEE-APS Topical Conf. Antennas Propag. Wireless Commun. (APWC)*, Sep. 2016, pp. 208–211.

[16] S. Mohamad, R. Cahill, and V. Fusco, "Performance of Archimedean spiral antenna backed by FSS reflector," *Electron. Lett.*, vol. 51, no. 1, pp. 14–16, Jan. 2015.

[17] M. Tanabe, M. Oyama, Y. Oishi, and Y. Masuda, "A spiral antenna over a high-impedance surface consisting of fan-shaped patch cells," in *Proc. IEEE-APS Topical Conf. Antennas Propag. Wireless Commun. (APWC)*, Sep. 2015, pp. 1596–1599.
[18] S. Mohamad, R. Cahill, and V. Fusco, "Selective high impedance surface active region loading of Archimedean spiral antenna," *IEEE Antennas Wireless Propag. Lett.*, vol. 13, pp. 810–813, 2014.
[19] H. Nakano, H. Oyanagi, and J. Yamauchi, "Spiral antenna above a composite HIS reflector," in *Proc. IEEE Antennas Propag. Soc. Int. Symp.*, Jul. 2010, pp. 1–4.
[20] D. Zeppettella and M. Ali, "A broadband directional circularly polarized spiral antenna on EBG structure," *J. Electromagn. Waves Appl.*, vol. 34, no. 11, pp. 1563–1585, 2020.
[21] M. Tanabe and H. Nakano, "Low-profile wideband spiral antenna with a circular HIS reflector composed of homogenous fan-shaped patch elements," *IEEE Trans. Antennas Propag.*, vol. 68, no. 10, pp. 7219–7222, Oct. 2020.
[22] M. Tanabe and H. Nakano, "Light-weight wideband spiral antenna with a two-layer circular HIS reflector: TL-CirHISR spiral antenna," *IET Microw., Antennas Propag.*, vol. 14, no. 14, pp. 1895–1901, Nov. 2020.
[23] H. Nakano, K. Kikkawa, N. Kondo, Y. Iitsuka, and J. Yamauchi, "Low-profile equiangular spiral antenna backed by an EBG reflector," *IEEE Trans. Antennas Propag.*, vol. 57, no. 5, pp. 1309–1318, May 2009.
[24] J. M. Bell and M. F. Iskander, "A low-profile Archimedean spiral antenna using an EBG ground plane," *IEEE Antennas Wireless Propag. Lett.*, vol. 3, pp. 223–226, 2004.
[25] D. Kim, C. Y. Park, Y. Kim, H. Kim, and Y. J. Yoon, "Four-arm sinuous antenna with low input impedance for wide gain bandwidth," *IEEE Access*, vol. 10, pp. 35265–35272, 2022, doi: 10.1109/ACCESS.2022.3163821.
[26] L.-L. Chen, L. Chang, Z.-Z. Chen, and Q.-N. Qiu, "Bandwidth-enhanced circularly polarized spiral antenna with compact size," *IEEE Access*, vol. 8, pp. 41246–41253, 2020.
[27] C. A. Balanis, *Antenna Theory: Analysis and Design*. Hoboken, NJ, USA: Wiley, 2005.
[28] A. Mohanty and S. Sahu, "Compact wideband hybrid fractal antenna loaded on AMC reflector with enhanced gain for hybrid wireless cellular networks," *AEU-Int. J. Electron. Commun.*, vol. 138, Aug. 2021, Art. no. 153837.
[29] M. Li, Q. L. Li, B. Wang, C. F. Zhou, and S. W. Cheung, "A low-profile dual-polarized dipole antenna using wideband AMC reflector," *IEEE Trans. Antennas Propag.*, vol. 66, no. 5, pp. 2610–2615, May 2018.
[30] M. A. Amiri, C. A. Balanis, and C. R. Birtcher, "Analysis, design, and measurements of circularly symmetric high-impedance surfaces for loop antenna applications," *IEEE Trans. Antennas Propag.*, vol. 64, no. 2, pp. 618–629, Feb. 2016.

DONGHYUN KIM received the B.S. degree in radio engineering from Chungnam National University, Daejeon, South Korea, in 2018. He is currently pursuing the integrated M.S. and Ph.D. degrees in electrical and electronic engineering with Yonsei University, Seoul. He has been a Research Assistant with Yonsei University, since 2018, where he has worked on antenna development for electronic warfare. His research interests include direction finding, artificial intelligence, and metamaterial. He was a recipient of the Best Student Paper Award, in 2021, IEEE ISAP and the Judge's Special Award in the Student Design Contest of International Symposium on Antennas and Propagation in Osaka, Japan, in January 2021.

CHAN YEONG PARK (Graduate Student Member, IEEE) received the B.S. degree in electronic engineering from Seokyeong University, Seoul, South Korea, in 2019. He is currently pursuing the integrated M.S. and Ph.D. degrees in electrical and electronic engineering with Yonsei University, Seoul. He has been a Research Assistant with Yonsei University, since 2019, where he has worked on antenna development for mm-wave applications. His research interests include holographic antenna and metasurface. He was a recipient of Best Paper Award, in 2021, KIEES Winter Conference and the Judge's Special Award in the Student Design Contest of International Symposium on Antennas and Propagation in Osaka, Japan, in January 2021.

CHANG-HYUN LEE received the M.S. and Ph.D. degrees in electronic information and communication engineering from Hongik University, Seoul, South Korea, in 2015 and 2020, respectively. He is currently a Research Engineer with LIG Nex1, Yongin, South Korea. His research interests include meta-structured antenna and ASAR RADAR.

YOUNG JOONG YOON (Senior Member, IEEE) received the B.S. and M.S. degrees in electronics engineering from Yonsei University, Seoul, South Korea, in 1981 and 1986, respectively, and the Ph.D. degree in electrical engineering from the Georgia Institute of Technology, Atlanta, GA, USA, in 1991. From 1992 to 1993, he was a Senior Researcher with the Electronics and Telecommunications Research Institute, Daejeon, South Korea. He joined Yonsei University as a Faculty Member, in 1993. He is currently a Professor with the Department of Electrical and Electronics Engineering. In 2011, he was the President of the Korean Institute of Electromagnetic Engineering and Science, Seoul. He has more than 30 years of extensive research and development experience in the fields of major interest in systems, such as ultrasonic, hyperthermia, high power antennas, electronic warfare antennas, and metasurface antennas.